The Atmospheric Chemistry of the Acetonoxy Radical

John J. Orlando* and Geoffrey S. Tyndall

Atmospheric Chemistry Division, National Center for Atmospheric Research, Boulder, Colorado 80303

Luc Vereecken* and Jozef Peeters

Department of Chemistry, KU Leuven, Celestijnenlaan 200F, B-3001, Heverlee, Belgium

Received: July 27, 2000; In Final Form: October 12, 2000

The chemistry of the acetonoxy radical, $CH_3C(O)CH_2O$, formed in the atmospheric degradation of acetone, was studied by a combination of experimental and theoretical methods. In an environmental chamber study conducted over the temperature range 225−298 K, acetonoxy radical chemistry was shown to be dominated by decomposition, $CH_3C(O)CH_2O \rightarrow CH_3C(O) + CH_2O$. No evidence was found for a reaction of this species with O_2, $CH_3C(O)CH_2O + O_2 \rightarrow CH_3C(O)CHO + HO_2$, even at 225 K in the presence of 1 atm O_2. In a theoretical ab initio and statistical kinetics investigation, the barrier to $CH_3C(O)CH_2O$ decomposition was found to be 6−7 kcal/mol. Using SSE theory and RRKM-based master equation analysis, it was determined that about 80% of the $CH_3C(O)CH_2O$ radicals formed in the $CH_3C(O)CH_2O_2 + NO$ reaction have sufficient energy to decompose "promptly" under tropospheric conditions. On the basis of TST theory and allowing for falloff, the dissociation rate of thermalized $CH_3C(O)CH_2O$ radicals was found to be on the order of 5×10^7 s^{-1} at 1 atm and 300 K and 5×10^5 s^{-1} at 0.2 atm and 220 K. The results confirm that the acetonoxy reaction with O_2 is always negligible in the troposphere, consistent with the experimental observations. As part of this study, the rate coefficient for reaction of Cl with acetone (k_2) was measured by a relative rate technique, and a value of $k_2 = (3.1 \pm 0.5) \times 10^{-11} \exp(-815 \pm 150/T)$ cm^3 $molecule^{-1}$ s^{-1} is reported.

Introduction

Acetone is one of the most abundant oxygenated organic compounds in the remote troposphere, with surface mixing ratios ranging from 500 to over 2000 pptv.[1] In the upper troposphere and the lower stratosphere, mixing ratios between 100 and 3000 pptv have been measured.[2−6] The global source strength of acetone has been estimated at 40 to 60 Tg/yr, about half of this originating from the atmospheric oxidation of hydrocarbons such as propane, isobutane, isobutene, and terpenes.[7,8] The estimated average atmospheric lifetime is on the order of 16 days, the major sinks being photolysis (estimated at ≈64% globally), reaction with OH radicals (≈24%), and deposition (≈12%).[4,7] In marine environments, especially during polar sunrise events,[9] the reaction with Cl atoms can also be of some importance.

As confirmed by direct measurements of OH and HO_2, photolysis of acetone constitutes an important source of HO_x in the dry upper troposphere and lower stratosphere (UTLS) via reactions of the products $CH_3 + CH_3CO$;[10,11] recent model calculations suggest a contribution of 20 to 40% to total HO_x in the dry UT.[12] Yet, in a recent determination of the rate coefficient of (R1) at low temperatures, Wollenhaupt et al. found that k_1 in the range $200 < T < 300$ K depends only slightly on temperature, decreasing from 1.8×10^{-13} cm^3 s^{-1} at $T = 298$ K to a minimum of 1.35×10^{-13} cm^3 s^{-1} at 240 K and increasing again to 1.5×10^{-13} cm^3 s^{-1} at $T = 200$ K. They conclude that, contrary to earlier assumptions, even in the UTLS ($T \approx 200$ K) the OH reaction should still be an important acetone sink, accounting for about 30% of the total loss.[13] These authors also report[14] the formation of CH_3 radicals, (R1b), occurring in parallel with the abstraction channel (R1a). From the above discussion, it is clear that the acetonyl radical, $CH_3C(O)CH_2$, is formed throughout the entire troposphere. Its subsequent chemistry appears to be of particular importance in the low-temperature and moderate-NO_x conditions of the UTLS, where it can affect to some extent the overall HO_x yield from acetone.

$$CH_3C(O)CH_3 + OH \rightarrow CH_3C(O)CH_2 + H_2O \quad (1a)$$

$$CH_3C(O)CH_3 + OH \rightarrow CH_3 + CH_3COOH \quad (1b)$$

The Cl-atom initiated oxidation of acetone has previously been investigated at 295−298 K in O_2−N_2 mixtures at pressures near atmospheric, both in the presence and the absence of NO_x.[15,16] These studies have shown that at room temperature the $CH_3C(O)CH_2O$ acetonoxy radicals resulting from the reaction of acetonylperoxy radicals with NO or from their self-reaction predominantly undergo decomposition, whereas the reaction with O_2 to form methylglyoxal is negligible.

$$CH_3C(O)CH_3 + Cl \rightarrow CH_3C(O)CH_2 + HCl \quad (2a)$$

$$CH_3C(O)CH_2 + O_2 + M \rightarrow CH_3C(O)CH_2O_2 + M \quad (2b)$$

$$CH_3C(O)CH_2O_2 + NO \rightarrow CH_3C(O)CH_2O^{(*)} + NO_2 \quad (3)$$

$$2\ CH_3C(O)CH_2O_2 \rightarrow 2\ CH_3C(O)CH_2O + O_2 \quad (4a)$$

$$\rightarrow CH_3C(O)CHO + CH_3C(O)CH_2OH + O_2 \quad (4b)$$

$$CH_3C(O)CH_2O \rightarrow CH_3C(O) + CH_2O \quad (5)$$

$$CH_3C(O)CH_2O + O_2 \rightarrow CH_3C(O)CHO + HO_2 \quad (6)$$

On the basis of these findings,[15,16] on an estimated rate coefficient for (R6) of $\approx 10^{-14}$ cm^3 $molecule^{-1}$ s^{-1}, and on an

* To whom correspondence should be addressed.

10.1021/jp0026991 CCC: $19.00
Published on Web 11/18/2000

estimated A-factor for (R5) of $\approx 10^{14}$ s^{-1}, one can estimate an upper limit of ≈10 kcal/mol for the barrier to decomposition of acetonoxy. The k_{th}(300 K) rate constant of about 10^6 s^{-1} recommended by Atkinson and Carter[17] for exothermic oxy radical decompositions implies a ≈9.5 kcal/mol barrier, consistent with the above. However, a barrier of this magnitude implies that at $T = 200-220$ K in the UTLS the thermal decomposition should become slower than reaction with O_2. Therefore, mechanistic/kinetic studies of the oxidation of acetonyl, both in the presence and the absence of NO, have to be extended to much lower temperatures, down to 200 K.

Furthermore, the chemistry of acetonoxy radicals resulting from (R3) is likely to be strongly affected or even dominated by a chemical activation effect, particularly at low temperature. As shown in recent studies,[18−23] substituted alkoxy radicals with a low dissociation barrier are subject to such an effect when they arise in an $RO_2 + NO$ reaction. The energy available from the exothermic $RO_2 + NO \rightarrow ROONO^* \rightarrow RO + NO_2$ reaction (exoergicity ≈ 11 kcal/mol for a primary RO_2 radical[24]) is partitioned over the reaction products such that a fraction of the oxy radicals is born with sufficient internal energy to decompose "promptly" (on a sub ns time scale), before collisional stabilization can occur. The oxy radicals that either arise with insufficient energy for dissociation or that suffer collisional energy loss before decomposition will be thermalized and can subsequently undergo either thermal decomposition or react with O_2. The effect will most likely apply to acetonoxy radicals, as their decomposition appears to involve a low barrier. As a result, in kinetic models the acetonylperoxy + NO reaction (R3) should rather be represented as a 2-channel process:

$$CH_3C(O)CH_2O_2 + NO \rightarrow CH_3C(O)CH_2O^* + NO_2 \quad (3a)$$

$$\rightarrow CH_3C(O)CH_2O + NO_2 \quad (3b)$$

where $CH_3C(O)CH_2O^*$ represents the sufficiently "hot" radicals that decompose promptly and $CH_3C(O)CH_2O$ represents the acetonoxy radicals that are thermalized before they react. The branching ratio for such a process shows some dependence on pressure as well as on temperature,[19−22] yet this T-dependence is much weaker than that of the rate of thermal dissociation, such that prompt dissociation may still be important or even dominant with respect to reaction with O_2 at temperatures too low for thermal dissociation. As an important consequence of the chemical activation effect, product data obtained for acetonoxy radicals originating from the peroxy self-reaction (R4) cannot be transposed to oxy radicals formed in (R3).

This paper reports on experimental and theoretical studies of the Cl-initiated oxidation of acetone in the temperature range of 220 to 300 K at near-atmospheric pressures, focusing in particular on the chemistry of the acetonoxy radical. The first major aim is to obtain quantitative information on the fate of the acetonoxy at lower temperatures from detailed oxidation product measurements under various conditions, both in the absence and in the presence of NO_x. To distinguish between the methylglyoxal production from the acetonoxy + O_2 reaction (R6) and from the peroxy self-reaction (R4b), product data have been collected over a wide range of O_2 pressures. Furthermore, to complement the experimental results, a detailed quantum chemical and theoretical kinetics study of the acetonoxy radical was carried out to quantify its thermal dissociation as well as its formation as a chemically activated species in (R3) and its subsequent prompt decomposition.

Experimental Section

All experiments were conducted using an environmental chamber/Fourier transform spectrometer (FTS) system, that has been described previously.[25] The stainless steel chamber is 2 m in length and has a volume of 47 L, and is interfaced to a Bomem DA3.01 FTS via a set of Hanst-type multipass optics, which provided an IR observational path length of 32.6 m. FTIR spectra were measured over the range 800−3900 cm^{-1} at a spectral resolution of 1 cm^{-1} and were typically obtained from the co-addition of 150−200 scans (≈3−4 min acquisition time). Experiments were conducted at temperatures ranging from 215 to 298 K. Chilled ethanol was circulated around the cell to control the gas temperature. Photolysis of the gas mixtures was conducted using a cw Xe-arc lamp, filtered to provide radiation between 235 and 400 nm. Minor components of gas mixtures were added to the chamber from smaller calibrated volumes, using a flow of N_2.

The rate coefficient for reaction of Cl atoms with acetone (R2) was determined using standard relative rate techniques,[26−30] with (R7) as the reference reaction:

$$Cl + CH_3C(O)CH_3 \rightarrow CH_3C(O)CH_2 + HCl \quad (2)$$

$$Cl + CH_2Cl_2 \rightarrow CHCl_2 + HCl \quad (7)$$

Measurements were made at temperatures ranging from 215 to 298 K. For these measurements, mixtures of Cl_2 ($\approx 1 \times 10^{16}$ molecule cm^{-3}), acetone ($5-10 \times 10^{14}$ molecule cm^{-3}), and CH_2Cl_2 ($6-14 \times 10^{14}$ molecule cm^{-3}) in 1 atm synthetic air were photolyzed, and the disappearance of acetone and CH_2Cl_2 was monitored by FTIR spectroscopy. The ratio of the rate coefficients k_2/k_7 was determined from the relative rates of decay using equation (A)

$$\ln\{[\text{acetone}]_o/[\text{acetone}]_t\} = k_2/k_7 \ln\{[CH_2Cl_2]_o/[CH_2Cl_2]_t\} \quad (A)$$

where $[\text{acetone}]_o$ and $[CH_2Cl_2]_o$ are the initial concentrations before reaction and $[\text{acetone}]_t$ and $[CH_2Cl_2]_t$ are the concentrations after varying reaction times.

For studies of the acetone oxidation mechanism, mixtures of Cl_2, acetone, NO (in some cases), O_2, and N_2 were photolyzed. Experiments were conducted over a range of conditions, as detailed later. On the basis of previous studies in our lab, photolysis of acetone oxidation products (e.g., formaldehyde and methylglyoxal) will be negligibly slow under the conditions employed. Oxidation products were quantified by means of spectral subtraction routines, using reference spectra previously obtained in our laboratory, except in the case of peracetic acid for which a separate set of calibration experiments was conducted. The peracetic acid sample was obtained (Aldrich) as a dilute peracetic acid/acetic acid solution in water. Vapors obtained from the sample were found to contain about 40 molar% H_2O, 35−40% acetic acid (calculated as equivalent monomer concentration), and 20−25% peracetic acid. Using a procedure similar to that described by Crawford et al.,[30] quantitative peracetic acid spectra were obtained following a proper accounting for the presence of acetic acid, H_2O, and acetic acid dimers. Acetic acid and water absorption cross sections used were determined in our laboratory, while the literature value for the acetic acid dimerization equilibrium constant, $K_{eq} = 2.5 \pm 0.3$ $Torr^{-1}$ was used.[30] The peracetic acid absorption cross section of $(5.3 \pm 0.7) \times 10^{-19}$ cm^2 $molecule^{-1}$ at 1295 cm^{-1} (base e) obtained is almost three times higher than that reported by Crawford et al.[30] The reason for the

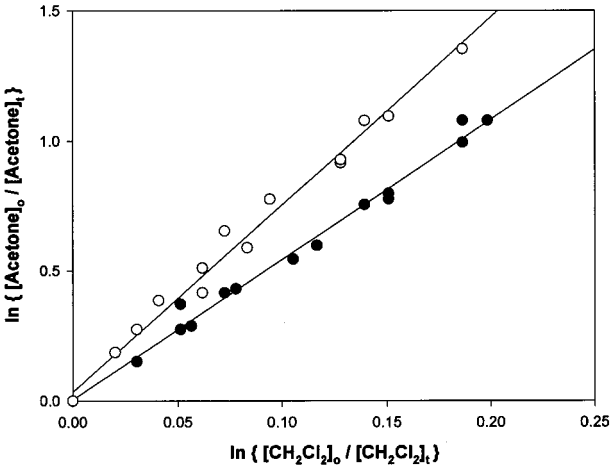

Figure 1. Plots of the decay of acetone versus CH_2Cl_2 at 295 K (solid circles) and 225 K (open circles) in the photolysis of Cl_2/acetone/CH_2Cl_2/air mixtures at 700 Torr total pressure.

discrepancy is not known, but may be related to an improper accounting for the presence of the H_2O impurity in the Crawford et al.[30] study. We note that this revised peracetic acid cross section has ramifications for the branching ratios reported by Crawford et al. in the reaction of $CH_3C(O)O_2 + HO_2$:

$$CH_3C(O)O_2 + HO_2 \rightarrow CH_3C(O)OOH + O_2 \quad (8a)$$

$$\rightarrow CH_3C(O)OH + O_3 \quad (8b)$$

Using the new cross section would lead to a revised value for $k_{8a}/k_8 = 0.72$, compared to the ratio $k_{8a}/k_8 = 0.88$ originally reported.[30] This revised value would be more in line with previous values of k_{8a}/k_8,[31−33] which range from 0.67 to 0.75.

Results and Discussion

(1) Kinetics of Cl Atom Reaction with Acetone. Initial experiments focused on the determination of the rate coefficent for (R2),

$$Cl + CH_3C(O)CH_3 \rightarrow CH_3C(O)CH_2 + HCl \quad (2)$$

data which were required for the quantitative interpretation of the Cl atom initiated acetone oxidation experiments to be discussed later. Measurements were made relative to (R7),

$$Cl + CH_2Cl_2 \rightarrow CHCl_2 + HCl \quad (7)$$

a reaction recently studied in our laboratory.[26] In that work, the Arrhenius expression $k_7 = 1.5 \times 10^{-11} \exp(-1100/T)$ was derived, based on an evaluation of our data and previous data. Sample relative rate data are shown in Figure 1, and all relative rate determinations and absolute values for k_2 are given in Table 1. These k_2 data are then plotted in Arrhenius form in Figure 2; linear least-squares fitting of these data to the Arrhenius equation yields $k_2 = (3.1 \pm 0.5) \times 10^{-11} \exp(-815 \pm 150/T)$ cm^3 molecule^{-1} s^{-1}, where the uncertainties include 2σ precision plus possible systematic errors and the uncertainty in the A-factor reflects the uncertainty in the room-temperature value.

Previous determinations of k_2 have been made only at room temperature. Wallington et al.[27] measured k_2 relative to the rate coefficient for reaction of Cl with ethyl chloride:

$$Cl + CH_3CH_2Cl \rightarrow CH_3CHCl + HCl \quad (9)$$

Using the most recent value for k_9, 8.6×10^{-12} cm^3 molecule^{-1} s^{-1},[28] a value of $k_2 = (2.5 \pm 0.2) \times 10^{-12}$ cm^3 molecule^{-1} s^{-1} is obtained, in reasonable agreement with our work ($k_2 = 2.0 \pm 0.3 \times 10^{-12}$ cm^3 molecule^{-1} s^{-1} at 298 K). Christensen et al.[29] have recently published relative rate data for k_2 using a number of reference species and report $k_2 = (2.2 \pm 0.4) \times 10^{-12}$ cm^3 molecule^{-1} s^{-1} at 298 K, also in agreement with our determination. The 298 K value obtained recently by Notario et al.[34] using a flash photolysis/ resonance fluorescence technique, $k_2 = (3.06 \pm 0.38) \times 10^{-12}$ cm^3 molecule^{-1} s^{-1}, is significantly higher than the recent relative rate determinations. Finally, we note that the IUPAC review panel[35] recommends a 298 K value of 3.5×10^{-12} cm^3 molecule^{-1} s^{-1} for k_2 based on the work of Wallington et al.,[27] but using an outdated value for k_9.

TABLE 1: Relative Rate Coefficient Data for Reaction of Cl with Acetone, Obtained Using the Reaction of Cl with CH_2Cl_2 as the Reference Reaction[a]

temp	measured k_2/k_7 (this work)	k_7 (ref 26)	k_2 (this work)
298	5.39	0.374	2.02
267	5.83	0.244	1.42
251	6.26	0.187	1.17
240	6.69	0.153	1.03
225	7.21	0.113	0.81
215	7.72	0.092	0.71

[a] Absolute rate coefficients are given in units of 10^{-12} cm^3 molecule^{-1} s^{-1} and are obtained using $k_7 = 1.5 \times 10^{-11} \exp(-1100/T)$ cm^3 molecule^{-1} s^{-1}.

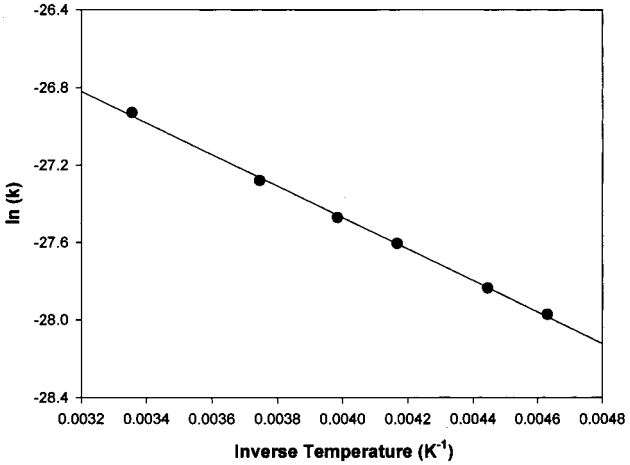

Figure 2. Arrhenius plot for k_2. Best fit to the data (solid line) is obtained for $k_2 = (3.1 \pm 0.5) \times 10^{-11} \exp(-815 \pm 150/T)$ cm^3 molecule^{-1} s^{-1}.

(2) Cl Atom Initiated Oxidation of Acetone. The primary goal of this series of oxidation experiments was to study the competition between reaction of the acetonoxy radical with O_2 (R6) and its thermal decomposition (R5), particularly at low temperature. This was achieved largely via the analysis of yields of CH_2O and methylglyoxal.

$$CH_3C(O)CH_2O \rightarrow CH_3C(O) + CH_2O \quad (5)$$

$$CH_3C(O)CH_2O + O_2 \rightarrow CH_3C(O)CHO + HO_2 \quad (6)$$

Experiments were conducted over a range of conditions, both in the presence of NO_x (298 K only) and in its absence (at temperatures between 225 and 298 K). For both the NO_x-containing and NO_x-free experiments, low ($\approx 10^{15}$ molecule cm^{-3}) and high ($\approx 2 \times 10^{16}$ molecule cm^{-3}) initial acetone concentrations were employed. The low acetone experiments

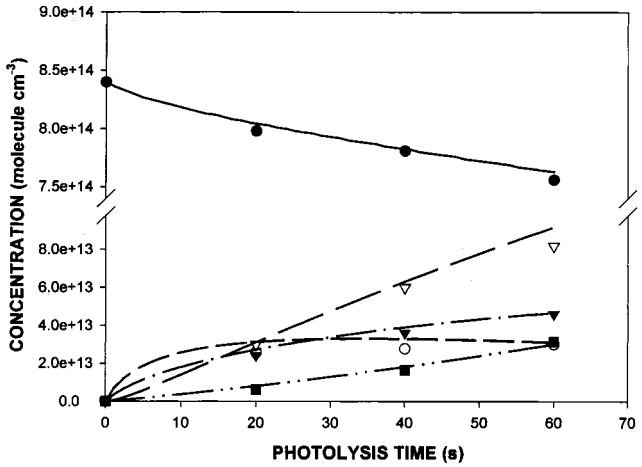

Figure 3. Observed (symbols) and modeled (lines) concentration profiles for a typical Cl_2/"low" acetone/NO/air experiment at 298 K. Solid circles: measured [acetone]. Open triangles: measured [CO]. Filled triangles: measured [CO_2]. Solid squares: measured [PAN]. Open circles: measured [CH_2O].

had the advantage of allowing one to follow both the acetone loss and product growth, though the rapid reaction of Cl with many of the key products (CH_2O and methylglyoxal, in particular) limited their steady-state levels, often to immeasurably small values. In the high acetone experiments, secondary reactions consuming the reaction products were minimized, but only immeasurably small fractional conversions of acetone occurred, such that mass balance could not be calculated. It was found that experiments conducted at high initial acetone levels and in the absence of NO_x, similar to those conducted by Jenkin et al.[15] at room temperature, were the most useful in the study of the competition between (R5) and (R6).

(a) Experiments Conducted in the Presence of NO_x. For the low acetone experiments, typical initial concentrations were as follows (in molecule cm^{-3}): Cl_2, $(8-20) \times 10^{15}$; acetone, $\approx 10^{15}$; NO, $\approx 7 \times 10^{14}$; O_2, $(0.4-2.2) \times 10^{19}$; N_2, $(1.3-2.0) \times 10^{19}$. Small amounts of NO_2 ($(2-3) \times 10^{13}$ molecule cm^{-3}) were typically present as well. Observed products in these experiments were CO, PAN, CO_2, and CH_2O, which accounted for 90 ± 15% of the acetone consumption (on a per carbon basis). No evidence was found for the presence of acetonyl nitrate or acetonyl peroxynitrate. Some sample data, showing acetone loss and product appearance versus photolysis time, are presented in Figure 3. No methylglyoxal was observed (detection limit $\approx 10^{13}$ molecule cm^{-3}), and hence there is no evidence for the occurrence of (R6).

Box model simulations of the reaction system were carried out with the Acuchem software package.[36] The full model consisted of about 110 reactions, the most important of which are given in Table 2 (stable products are shown in bold type). Note that destruction of acetone, CH_2O and $CH_3C(O)CHO$ (if formed) leads to the production of HO_2 which in the presence of NO generates OH. However, modeling studies indicate that only about 5% of the acetone oxidation will actually be initiated by OH in these experiments. For initial simulations, it was assumed that all acetonoxy radicals decompose (either via chemical activation or following collisional thermalization), and that reaction with O_2 is negligible. The actual decomposition mechanism is not crucial to the modeling, as even the slower thermal decomposition is not rate-limiting. Modeled temporal profiles of acetone and its oxidation products agree very well (to within ±10%) with those measured, as shown in Figure 3. Further simulations were then run to determine the extent of occurrence of (R6) that would still be consistent with the observations (i.e., the lack of detection of methylglyoxal and the observed steady-state level of CH_2O). The lack of detection of methylglyoxal does not provide a stringent limit; as many as 35% of the acetonoxy radicals could be reacting with O_2 before the methylglyoxal would reach observable levels. CH_2O model/measurement comparisons, however, do provide a more stringent test. It is estimated that no more than 20% of the acetonoxy radicals could be reacting with O_2 before modeled levels of CH_2O became significantly lower than those measured.

For the high acetone experiments, initial concentrations were as follows (in molecule cm^{-3}): Cl_2, $13-22 \times 10^{15}$; acetone, $(1-2) \times 10^{16}$; NO, $10-20 \times 10^{14}$; O_2, 2.1×10^{19}; N_2, $1.8-3.2 \times 10^{18}$, with small amounts of NO_2, $(5-7) \times 10^{13}$, also present. Models show that only a small portion of the chemistry (≈10%) is initiated by OH under these conditions. The products observed in these experiments were the same as those observed in the low acetone experiments above, namely, CO, PAN, CO_2, and CH_2O. Again, no methylglyoxal was observed ($< 3 \times 10^{13}$ molecule cm^{-3}). As was the case in the low acetone experiments just discussed, box modeling studies of these reaction conditions allow us to place an upper limit of 20% on the fraction of acetonoxy radicals reacting with O_2 in 1 atm O_2.

(b) Experiments Conducted in the Absence of NO. The finding that the decomposition of acetonoxy dominates over its reaction with O_2 at 298 K is consistent with the results of Jenkin et al.,[15] who reported $k_5/(k_6\,[O_2]) > 10$ in 1 atm O_2 and in the absence of NO_x. Our findings are also consistent with the work of Sehested et al,[37] who observed PAN as a product of the thermal decomposition of acetonylperoxy nitrate, even at 250 K:

$$CH_3C(O)CH_2O_2NO_2 \rightarrow CH_3C(O)CH_2O_2 + NO_2 \quad (32)$$

$$CH_3C(O)CH_2O_2 + NO \rightarrow CH_3C(O)CH_2O + NO_2 \quad (3)$$

$$CH_3C(O)CH_2O\ (+\,O_2) \rightarrow CH_3C(O)O_2 + CH_2O \quad (5)$$

$$CH_3C(O)O_2 + NO_2 \rightarrow CH_3C(O)O_2NO_2\ (PAN) \quad (15)$$

However, as will be shown later, the majority of the acetonoxy dissociation in the presence of NO_x occurs as the result of chemical activation, making direct comparison of the NO_x-free and NO_x-containing experiments complicated and hindering our ability to study the chemistry of the thermalized acetonoxy radicals. Thus, further experiments (with an emphasis on lower temperatures) were carried out in the absence of NO_x where chemical activation does not occur.

Experiments were conducted under conditions of low (≈10^{15} molecule cm^{-3}) and high (≈10^{16} molecule cm^{-3}) initial acetone concentrations, at temperatures ranging from 225 to 298 K. A typical low acetone experiment involved the photolysis of a mixture of Cl_2 ($\approx 1 \times 10^{16}$ molecule cm^{-3}) and acetone ($\approx 1 \times 10^{15}$ molecule cm^{-3}) in 1 atm synthetic air. At 298 K, the observed products were CO, CO_2, CH_2O, $CH_3C(O)OH$, $CH_3C(O)OOH$, CH_3OH, and HCOOH, which accounted for 70 ± 15% of the acetone carbon consumed. Methylglyoxal and hydroxyacetone, expected from the self-reaction of the acetonyl peroxy radicals, are below the detection limit of $(2-3) \times 10^{13}$ molecule cm^{-3} but may account for a nonnegligible fraction of the missing carbon. Furthermore, the hydroperoxides expected to be formed in these experiments, CH_3OOH and $CH_3C(O)CH_2$-OOH, are typically very unstable in our chamber, and their loss at the cell walls may also account for some of the missing carbon.

TABLE 2: Major Reactions Used in Simulations of Acetone Oxidation[a]

reaction				k_{298}	k_{225}
(2)	$Cl + CH_3C(O)CH_3$	→	$CH_3C(O)CH_2 + HCl$	2.1e-12	8.3e-13
(10)	$CH_3C(O)CH_2 + O_2$	→	$CH_3C(O)CH_2O_2$	7.5e-11	7.5e-11
(3)	$CH_3C(O)CH_2O_2 + NO$	→	$CH_3C(O)CH_2O^* + NO_2$	8e-12	9e-12
		→	$CH_3C(O)CH_2O + NO_2$		
(11)	$CH_3C(O)CH_2O^*$	→	$CH_3C(O) + \mathbf{CH_2O}$	rapid	rapid
(5)	$CH_3C(O)CH_2O$	→	$CH_3C(O) + \mathbf{CH_2O}$	variable	variable
(6)	$CH_3C(O)CH_2O + O_2$	→	$CH_3C(O)CHO + HO_2$	9.7e-15	1e-14
(12)	$CH_3C(O) + O_2$	→	$CH_3C(O)O_2$	5e-11	5e-11
(13)	$CH_3C(O)O_2 + NO$	→	$CH_3O_2 + \mathbf{CO_2} + NO_2$	1.8e-11	2.6e-11
(14)	$CH_3O_2 + NO\ (+ O_2)$	→	$NO_2 + HO_2 + \mathbf{CH_2O}$	7.7e-12	1e-11
(15)	$CH_3C(O)O_2 + NO_2$	→	PAN	9e-12	1.3e-11
(16)	$Cl + CH_2O$	→	$Cl + HCO$	7.3e-11	7.3e-11
(17)	$HCO + O_2$	→	$HO_2 + \mathbf{CO}$	5.5e-12	6.5e-12
(18)	$Cl + CH_3C(O)CHO$	→	$CH_3C(O) + \mathbf{CO} + HCl$	4.8e-11	4.8e-11
(19)	$HO_2 + NO$	→	$OH + NO_2$	8.1e-12	1.1e-11
(20)	$OH + CH_3C(O)CH_3$	→	$CH_3C(O)CH_2$	2.2e-13	1.0e-13
(4)	$CH_3C(O)CH_2O_2 + CH_3C(O)CH_2O_2$	→	$CH_3C(O)CH_2O + CH_3C(O)CH_2O + O_2$	6.0e-12	4.5e-12
		→	$\mathbf{CH_3C(O)CHO} + \mathbf{CH_3C(O)CH_2OH} + O_2$	2.0e-12	4.5e-12
(21)	$CH_3C(O)CH_2O_2 + CH_3C(O)O_2$	→	$CH_3C(O)CH_2O + CH_3 + CO_2 + O_2$	1.0e-11	1e-11
		→	$\mathbf{CH_3C(O)CHO} + \mathbf{CH_3C(O)OH} + O_2$	1.0e-12	1e-12
(22)	$CH_3C(O)CH_2O_2 + HO_2$	→	$\mathbf{CH_3C(O)CH_2OOH} + O_2$	9.0e-12	1.5e-11
(8)	$CH_3C(O)O_2 + HO_2$	→	$\mathbf{CH_3C(O)OH} + O_3$	3.0e-12	1.8e-11
		→	$\mathbf{CH_3C(O)OOH} + O_2$	9.0e-12	1.8e-11
(23)	$CH_3O_2 + HO_2$	→	CH_3OOH	5.6e-12	1.4e-11
(24)	$CH_3O_2 + CH_3O_2$	→	$CH_3O + CH_3O + O_2$	1.6e-13	0.7e-13
		→	$\mathbf{CH_3OH} + \mathbf{CH_2O} + O_2$	3.2e-13	5.1e-13
(25)	$CH_3O_2 + CH_3C(O)O_2\ (+ O_2)$	→	$CH_3O + CH_3O_2 + \mathbf{CO_2} + O_2$	1.2e-11	2e-11
		→	$CH_2O + CH_3C(O)OH + O_2$	1.2e-12	2e-12
(26)	$CH_3C(O)O_2 + CH_3C(O)O_2\ (+ 2\ O_2)$	→	$2\ CH_3O_2 + 2\ \mathbf{CO_2} + O_2$	1.7e-11	2.7e-11
(27)	$CH_3O_2 + CH_3C(O)CH_2O_2$	→	$CH_3O + CH_3C(O)CH_2O$	1.1e-12	0.6e-12
		→	$\mathbf{CH_3OH} + \mathbf{CH_3C(O)CHO} + O_2$	1.4e-12	2.8e-12
		→	$\mathbf{CH_2O} + \mathbf{CH_3C(O)CH_2OH} + O_2$	1.4e-12	2.8e-12
(28)	$HO_2 + HO_2$	→	$H_2O_2 + O_2$	3.0e-12	7.5e-12
(29)	$HO_2 + HCOOH$	↔	adduct → HCOOH	1e-13,50,10	
(30)	$CH_3O + O_2$	→	$CH_2O + HO_2$	1.9e-15	6.5e-16
(31)	$Cl_2 + h\nu$	→	$Cl + Cl$	3e-4 s^{-1}	3e-4 s^{-1}

[a] The full model included 110 reactions. Rate coefficients in cm^3 $molecule^{-1}s^{-1}$.

The chemistry occurring in this NO_x-free system is quite complicated, due to the occurrence of the peroxy radical self- and cross-reactions.[15,16,35,38,39] Under conditions of low acetone, reactions of the various peroxy radicals with Cl atoms[40] and ClO[41] are also expected to occur. Box model simulations of the chemistry were conducted using the full mechanism, portions of which are given in Table 2. Rate coefficients were taken from IUPAC[35] and NASA[38] evaluations, when available, with acetonylperoxy radical rate coefficients taken from the work of Bridier et al.[16] Rate coefficients employed for the reaction of Cl and ClO with acetonylperoxy were based on the corresponding CH_3O_2 reactions.[38,40,41]

Initial modeling efforts were conducted under the assumption that thermal decomposition dominates the chemistry of the acetonoxy radical. The model was able to reproduce the observations quite well, especially when the large uncertainty in the RO_2/RO_2 and Cl/RO_2 reaction rates and mechanisms is considered. Figure 4 gives a model/measurement comparison for one experiment, with only the major products shown. Much like in the low acetone experiments carried out in the presence of NO_x, the inability to detect methylglyoxal is not a sensitive diagnostic of the acetonoxy chemistry under these conditions. Based on a comparison of the modeled and measured CH_2O concentration profiles over a range of conditions, however, a lower limit $k_5/k_6 > 5 \times 10^{19}$ molecule cm^{-3} can be determined, consistent with (but less informative than) the lower limit reported by Jenkin et al.,[15] $k_5/k_6 > 2 \times 10^{20}$ molecule cm^{-3}.

Similar experiments were carried out at 225 K. Products observed were the same as at room temperature, CO, CO_2, CH_2O, $CH_3C(O)OOH$, $CH_3C(O)OH$, CH_3OH, and HCOOH.

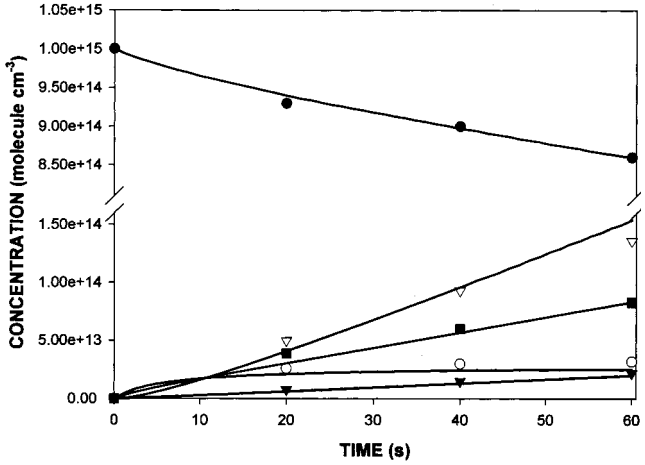

Figure 4. Observed (symbols) and modeled (lines) concentration profiles for a typical Cl_2/low acetone/air experiment at 298 K. Solid circles: measured [acetone]. Open triangles: measured [CO]. Solid squares: measured [CO_2]. Open circles: measured [CH_2O]. Filled triangles: measured [$CH_3C(O)OOH$].

Minor amounts of $CH_3C(O)Cl$ were also observed in experiments conducted at low [O_2]:

$$CH_3C(O) + Cl_2 \rightarrow CH_3C(O)Cl + Cl \qquad (33)$$

The carbon-balance in these experiments was similar to room temperature, 81 ± 15%, with the shortfall again likely due to the inability to detect methylglyoxal, hydroxyacetone, and the

hydroperoxide species. In addition, an as yet unidentified absorption feature at 1290 cm^{-1} was detected. For low-temperature modeling, rate coefficients and branching ratios for the reactions of the acetonylperoxy radical with HO_2 and other peroxy radicals were estimated from available data on the analogous CH_3O_2 reactions (see Table 2 for rate coefficients used). The model/measurement agreement is quite good (quantifiable products agree to within ±25%) with one exception: the model overpredicts the levels of acetic and peracetic acid by about 50−100%. This may be the result of an unidentified loss for the acids at low temperature, or it may be due to incorrect parameterization of acetylperoxy radical chemistry in the model. Nonetheless, based on the measured levels of CH_2O and the lack of any dependence on $[O_2]$, box modeling studies of these reaction conditions suggest $k_5/k_6 > 2 \times 10^{19}$ molecule cm^{-3}. Though a more stringent constraint on the k_5/k_6 ratio will be determined below, this lower limit is sufficient to show that decomposition (R5) will be the major fate of acetonoxy radicals in the upper troposphere.

Experiments with high initial acetone involved the photolysis of mixtures of Cl_2 ($7-20 \times 10^{15}$ molecule cm^{-3}), acetone ($15-25 \times 10^{15}$ molecule cm^{-3}), O_2 (50−650 Torr) and N_2 (balance) at a pressure of 1 atm. These experiments were conducted at temperatures ranging between 225 and 298 K. Products observed in all cases were CO, CO_2, CH_3OH, HCOOH, CH_2O, $CH_3C(O)OH$, methylglyoxal, acetyl chloride (low $[O_2]$ only), and hydroxyacetone, though the high acetone concentration obscures various regions of the IR, making the quantification of acetic acid and the detection of peracetic acid difficult. The unidentified absorption feature at 1290 cm^{-1} was also present. To study the competition between (R5) and (R6) in the most direct fashion possible, back-to-back experiments were conducted with identical Cl_2 and acetone concentrations, but with the O_2 partial pressure varied from 50 to 650 Torr. In all cases, at all temperatures, no significant change in any product concentration was observed with the variation of the O_2 pressure (including methylglyoxal, for which a 25% change would be detectable). Thus, we have no evidence for a reaction of the acetonoxy radical with O_2 under any conditions, even in 1 atm O_2 at 225 K.

To provide a lower limit for the ratio of k_5/k_6, box model simulations were carried out. For room temperature, under the assumption that all acetonoxy radicals decompose, the model was able to reproduce the concentrations of all quantifiable species to better than ±20%. The model was then run with various k_5/k_6 ratios, at high (650 Torr) and low (50 Torr) O_2. It was found that for $k_5/k_6 = 1.5 \times 10^{20}$ molecule cm^{-3}, a 25−30% increase in methylglyoxal and a ≈15% decrease in CH_2O would have occurred between the high and low O_2 experiments, changes that would have been detectable. These experiments are essentially identical to those carried out at room temperature by Jenkin et al.,[15] who also observed that the temporal profiles of formaldehyde and methylglyoxal were independent of O_2. Their modeling study suggested a lower limit for k_5/k_6 of 2×10^{20} molecule cm^{-3}, very similar to our limit.

The same procedure was used at 225 K, running the model at various k_5/k_6 at high and low O_2 partial pressures. For $k_5/k_6 = 1 \times 10^{20}$ molecule cm^{-3}, a 30% increase in methylglyoxal (and a 15% decrease in CH_2O) is expected between the 50 Torr O_2 and 650 Torr O_2 experiments, which should have been observable. This lower limit for k_5/k_6 allows for an estimate of the barrier height for acetonoxy decomposition. First, we assume a value for $k_6 = 9 \times 10^{-15}$ cm^3 molecule^{-1} s^{-1} at 225 K, by analogy to reaction of 1-propoxy with O_2,[35,42] which leads to the conclusion that $k_5 > 0.9 \times 10^6$ s^{-1}. This fact, coupled with an A-factor of $\approx 10^{13}$ s^{-1} (typical for alkoxy radical decompositions),[43−45] implies an activation energy for decomposition of no more than 7.5 kcal/mol. As will be made apparent in the following sections, this upper limit is entirely consistent with the barrier height estimated by theoretical methods, 6−7 kcal/mol.

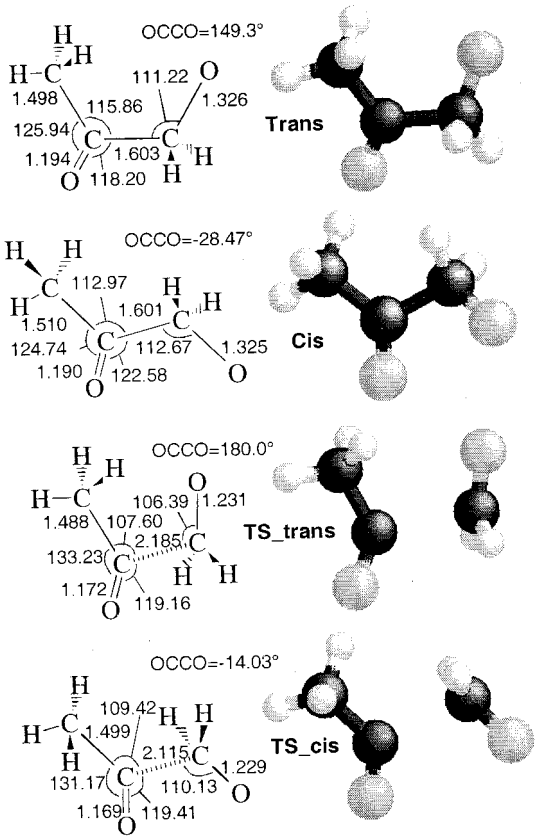

Figure 5. Selected geometric parameters for the acetonoxy rotamers and their transition states for C−C bond rupture. Bond lengths are in angstroms, angles in degrees.

(3) Quantum Chemical Characterization. Geometry optimizations and vibration frequency calculations for the acetonylperoxy radical rotamers, the acetonylperoxynitrite intermediate, the acetonoxy radical rotamers, and the transition states for C−C bond rupture of the acetonoxy radical were performed at the B3LYP-DFT level of theory as implemented in the Gaussian 98 program suite,[46] using the 6-31G(d,p) basis set. This level of theory was already validated in earlier studies[20−22] to give barrier heights for dissociation of C_3-C_4 alkoxy radicals and the β-hydroxyethoxy radical within 0.5 kcal/mol of the available direct experimental data, indicating that this level of theory is reliable for the task at hand.

The acetonylperoxy radicals and acetonoxy radicals have several degrees of freedom for internal rotation and can exist in different rotameric forms differing in the O−C−C−O and, if applicable, the C−C−O−O dihedral angles. As shown in Figure 5 and Table 3, two rotamers with a corresponding enantiomer each were found for the acetonoxy radicals, with O−C−C−O dihedral angles of 150° and 25°, with the relative energy of the latter rotamer higher by 4.0 kcal/mol. The geometries, relative energies, and vibrational frequencies of the rotamers are essentially unchanged when repeating the calculations using a 6-311++G(2df,2pd) basis set, indicating convergence at the B3LYP-DFT level of theory with respect to the basis set. For the acetonylperoxy radicals, we found four

TABLE 3: Zero-Point Energy Corrected Relative Energies for the Rotamers of the Acetonoxy Radicals and Their Transition States for C−C Bond Rupture, the Acetonylperoxy Radicals and the 3-Hydroperoxyacetonyl Radicals at Various Levels of Theory

structure	energy hartree	ZPE kcal/mol	OCCO angle	CCOO angle	E_{rel} kcal/mol
		CH_3COCH_2O			
B3LYP-DFT/6-31G(d,p)					
trans	−267.6985901	45.3[a]	150.5°		0.00
TS_trans	−267.6860115	43.7[a]	180.0°		6.37
cis	−267.6915636	46.7[a]	25.3°		4.03
TS_cis	−267.6792748	43.7[a]	16.3°		10.53
B3LYP-DFT/6-311++G(2df,2pd)					
trans	−267.7995099	46.8	149.3°		0.00
TS_trans	−267.7904611	45.3	180.0°		4.22
cis	−267.7926983	46.5	28.5°		4.00
TS_cis	−267.7841703	45.2	14.0°		8.22
CCSD(T)/6-31+G(d,p) // B3LYP-DFT/6-311++G(2df,2pd)					
trans	−266.9847109	46.8[b]			0.00
TS_trans	−266.9713680	45.3[b]			6.91
		CH_3COCH_2OO			
B3LYP-DFT/6-31G(d,p)					
tp	−342.8616577	48.6[a]	178.8°	79.1°	0.00
tt	−342.8596117	48.4[a]	179.7°	179.5°	1.06
mp	−342.8584381	48.5[a]	−3.9°	75.8°	1.93
mt	−342.8566964	48.3[a]	−4.4°	178.8°	2.81
		CH_2COCH_2OOH			
B3LYP-DFT/6-31G(d,p)					
CH_2COCH_2OOH	−342.8402339	47.8[a]	187.8°	69.9°	12.57
H-shift TS	−342.8129358	45.1[a]	187.3°	54.2°	26.89

[a] Scaled by 0.9614 (ref 47). [b] Values obtained at B3LYP-DFT/6-311++G(2df,2pd) level.

different rotamers with relative energies and geometries in agreement with earlier calculations on the β-hydroxyalkoxy radical.[20−22]

The kinetic calculations described later are most sensitive to the characteristics of the transition state (TS) for β C−C bond rupture of the acetonoxy radicals, shown in Figure 5 and listed in Table 3. Again, the B3LYP-DFT/6-31G(d,p) barrier height, 6.4 kcal/mol, is in keeping with the experimentally derived upper limit of 7.5 kcal/mol (see earlier). As was already found for other β-substituted alkoxy radicals, the different rotamers have comparable transition state barriers to dissociation. The optimizations of the transition states were repeated using the 6-311++G(2df,2pd) basis set, but it is known that at this level of theory one tends to find too low a barrier height for (substituted) alkoxy radicals compared to the experimental data,[48] such that the barrier height derived at that level of theory, 4.2 kcal/mol, should be considered a lower limit. The reason for this trend is unknown; geometries and vibrational frequencies are not affected. We also performed single point CCSD(T)/6-31+G(d,p) calculations on the DFT/6-311++G(2df,2pd) geometries, finding a barrier height of 6.9 kcal/mol, in fair agreement with the DFT/6-31G(d,p) result. Because the basis set used is somewhat small for use in CCSD(T) calculations, we consider this value to be an upper limit estimate for the barrier height. We also attempted to perform G2 and G3 calculations, but found that the MP2 geometries are too sensitive to the basis set used: e.g., for the lowest acetonoxy rotamer we find an O−C−C−O angle of 179.9° for the 6-31G(d) basis set, 165° for 6-31G(d,p), and 161° for 6-31G(2df,p). Obviously, this invalidates the use of single-point calculations at varying levels of theory and basis sets based on any MP2 geometry, as is done in the G2 and G3 methods. The geometry found using MP2 tends toward the B3LYP-DFT geometry with increasing basis set size, indicating that the DFT geometries are good estimates. The difference in basis set superposition error (BSSE) between minima and their transition states is usually small; we therefore did not make explicit correction for BSSE.

As discussed in more detail later, the acetonylperoxynitrite intermediate (ROONO) has a fairly short lifetime, and the characteristics of this intermediate, as well as those of the transition states for its dissociation to NO + RO_2 and NO_2 + RO, have only a small effect on the RO decomposition results obtained in the next section. We therefore chose not to perform a full microvariational treatment of the barrierless ROONO dissociation channels, and instead approximated these transition states by a constrained optimization at a bond length of 2.4 Å for the breaking bond. The lifetime of the acetonylperoxynitrite intermediate is sufficiently long to ensure a steady state distribution between its different internal rotamers, making it unnecessary to explicitly take the different rotamers of the acetonylperoxy radicals and of the acetonylperoxynitrite intermediate into account.

Finally, we also examined the possibility of a 1,5-H shift of a methyl-hydrogen in the acetonylperoxy radicals, forming 3-hydroperoxyacetonyl radicals ($CH_2C(O)CH_2OOH$, "QOOH") which might react subsequently with O_2 to form a new peroxy radical. At the B3LYP-DFT/6-31G(d,p) level of theory, this rearrangement, for the most stable rotamer, is found to be endoergic by 12.5 kcal/mol and to face an energy barrier of 26.9 kcal/mol. According to these results, the thermal isomerization is expected to be negligibly slow under all atmospheric conditions (rate $< 10^{-7}$ s^{-1}) compared to the usual peroxy radical reactions with NO, HO_2 etc. Yet, one also needs to consider the "prompt" isomerization of the nascent peroxy radicals, which contain an excess energy of some 30 to 35 kcal/mol,[24] and thus lie above the isomerization barrier. An RRKM estimate puts the rate of the prompt isomerization $RO_2^* \rightarrow$ QOOH* at the initial energy content at only $\approx 10^6$ s^{-1}, which is much slower than the rate of collisional stabilization of $\approx 10^9$ s^{-1}. Therefore, isomerization to QOOH should be negligible.

(**4) Kinetics of "Prompt" and Thermal Decomposition of Acetonoxy Radicals: Theoretical Quantification.** The first part of this section describes the theoretical quantification of the fraction of acetonoxy radicals formed in (R3) that dissociate

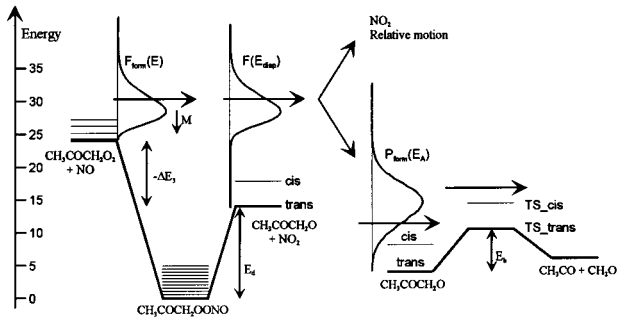

Figure 6. Reaction scheme for acetonoxy radicals formed in the reaction of acetonylperoxy radicals with NO. Energies are in kcal/mol, with $-\Delta E_3 = 10.5$ kcal/mol, $E_d = 14$ kcal/mol, $E_b = 6.9$ kcal/mol (upper limit). $F_{form}(E)$ is the nascent energy distribution for the acetonylperoxynitrite radicals, $F(E_{disp})$ is their energy distribution at dissociation. $P_{form}(E_A)$ is the nascent energy distribution for the acetonoxy radicals formed in (R3).

"promptly", i.e., before collisional stabilization. The quantum statistics based methodologies, as implemented in our URESAM-3 program suite,[49] have been described at length in earlier work, where they were applied to similar processes of β-hydroxyethoxy and β-hydroxypropoxy radicals formed in the oxidation of ethene and propene, respectively, resulting in theoretical predictions in excellent agreement with the observations.[20−22] Here, only the outlines of the methodologies will be given, together with the results.

The sequence of events leading to prompt dissociation of the oxy radicals is illustrated schematically by the potential energy and energy distribution diagram of Figure 6. Four steps can be discerned in this sequence: (i) reaction of $CH_3C(O)CH_2O_2$ with NO to form an activated peroxynitrite ROONO* with an internal energy distribution at formation, $F_{form}(E_{th})$, inherited from the thermal reactants; (ii) collisional energy loss of the ROONO* prior to its dissociation into RO + NO_2, which modifies its internal energy distribution to $F_{diss}(E)$ at dissociation; (iii) dissociation of the ROONO* and partitioning of the disposable excess energy, E_{disp}, over the two fragments and over the degrees of freedom of their relative motion, resulting in a given internal energy distribution function $P_{form}(E_A)$ of the RO fragment; (iv) prompt unimolecular dissociation of the resulting chemically activated oxy radicals, in competition with their collisional thermalization. Each of the steps above was treated theoretically and quantified, as briefly discussed below.

(i) The thermal internal energy distribution $F_{form}(E_{th})$ of formation of the chemically activated peroxynitrite $CH_3C(O)CH_2OONO^*$ from $CH_3C(O)CH_2O_2$ + NO was derived from the sum of states $G^{\neq}(E - E_0)$ of the (variational) entrance transition state,[50] based on the vibration frequencies obtained in a quantum chemical characterization at a separation of 2.4 Å, as discussed earlier. The form of the distribution function $F_{form}(E_{th})$ is shown in Figure 6. The thermal energy distribution, with an average value $\langle E_{th} \rangle$ of 4.9 kcal/mol at 300 K, is superimposed on the chemical activation energy, i.e., the well depth with respect to the reactants.

(ii) The internal energy distribution function of the ROONO* at dissociation, $F_{diss}(E)$, as modified by collisions during its lifetime, was obtained by an RRKM-based master equation (ME) analysis of the dissociation of ROONO* in competition with collisional energy transfer to the bath gas. The ROONO* dissociation rate and hence also the collisional energy losses depend on the internal energy E (see sub **i**), on the energy E_d of dissociation to RO + NO_2, and on the vibrational characteristics of the (variational) transition state (TS) for dissociation. There is no barrier in the exit channel for this process.[51] The various quantities involved are not critical because collisional energy losses are small here; the vibrational frequencies of the exit TS were again obtained in a quantum chemical characterization at a breaking bond length of 2.4 Å. The ROONO → RO + NO_2 dissociation energy E_d was taken equal to 14 kcal/mol as for the analogous 2-butyl case;[51] for the overall exoergicity $\Delta E_3(0\ K)$ of the RO_2 + NO → RO + NO_2 reaction, a value of 10.5 kcal/mol was adopted, between the values for the analogous ethyl- and isopropylperoxy reactions.[24] Collisional energy transfer was described in the ME equation by Troe's biexponential model,[52] with an average energy transferred per collision $\langle \Delta E_{tot} \rangle$ of -150 cm^{-1}. The RRKM-ME analysis revealed collisional energy losses before dissociation to RO + NO_2 to be negligible. The energy distribution at dissociation, $F_{diss}(E)$, resulting from the ME analysis is also depicted in Figure 6, for $T = 300$ K and 1 atm pressure. The average ROONO* lifetime for reactants at 300 K is about 10^{-10} s, long enough to ensure complete statistical distribution of the total internal energy over all internal modes. Formation of organic nitrate appears to be negligible here and need not be considered.

(iii) When the ROONO* dissociates, the disposable excess internal energy E_{disp} above the dissociation limit is imparted to the separating fragments. The E_{disp} can be seen as the overall exoergicity $-\Delta E_3(0\ K) = 10.5$ kcal/mol, increased by the thermal energy of formation of the peroxynitrite and decreased by the collisional energy losses during the ROONO* lifetime. The distribution $F(E_{disp})$ is identical to the $F_{diss}(E)$ function derived above (sub **ii**), but shifted downward by the ROONO → RO + NO_2 dissociation energy E_d of 14 kcal/mol. As shown earlier,[20−22] the contribution of rotational energy of the initial ROONO* to the internal energy available to the reaction products can be neglected. As the lifetime of the ROONO* is long enough ($\approx 10^{-10}$ s) for a statistical distribution of its internal energy over all its internal degrees of freedom, the excess energy E_{disp} should likewise be partitioned fully statistically over the separating fragments and their degrees of freedom of relative motion (i.e., the "transition" modes). The energy partitioning was quantified using the extended separate statistical ensemble (SSE) theory,[53] suitable for a dissociation process through a barrierless exit channel and involving a late and loose transition state. The theory and its extension as well as the conditions for its applicability have already been discussed in depth earlier.[20−22] In essence, SSE theory evaluates the partitioning of E_{disp} by adopting equal probabilities for each discrete internal quantum state of the (nearly) dissociated molecule. In this way, the available energy is distributed over the acetonoxy radical, the NO_2 fragment and the six degrees of freedom (d.f.) of relative motion in accordance with the respective relative increases of the densities of states $N(E)$ with energy. The nonnormalized probability $P_{A_i}^{E_{disp}}(E_A)$ of forming an acetonoxy fragment A in rotameric form i with energy E_A (the energy above the zero point level of the most stable rotamer) for a given total energy E_{disp} available to the products can be expressed as:

$$P_{A_i}^{E_{disp}}(E_A) = N_{A_i}(E_A) \times \int_0^{E_{tot}-E_A} [N_{NO_2}(E_{NO_2}) \times N_{rel.mot.}(E_{tot} - E_A - E_{NO_2})] dE_{NO_2}$$

Normalization requires dividing by the sum of this expression over all acetonoxy rotamers integrated over all energies E_A from 0 to E_{disp}. For the acetonoxy and NO_2 fragments the $N(E)$ were obtained by exact count using the DFT rovibrational data,

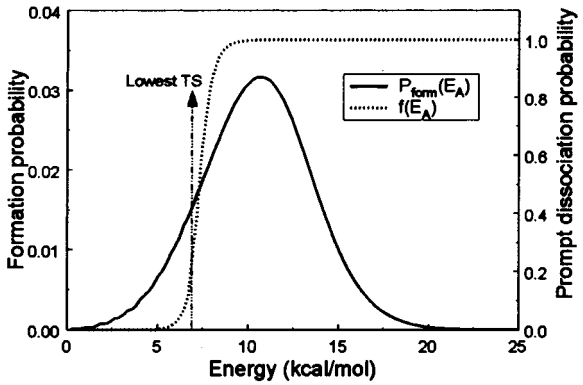

Figure 7. Predicted nascent vibrational energy distribution $P_{form}(E_A)$ for the acetonoxy radicals formed in (R3) at 300 K (energy grain size = 0.239 kcal/mol). Predicted probability $f(E_A)$ of prompt dissociation at 300 K and 1 atm.

TABLE 4: Predicted Prompt Dissociation Fraction for the Acetonoxy Radicals Formed in (R3), at Different Temperatures and Pressures, Calculated Using a Barrier Height to Dissociation of 6.9 Kcal/Mol[a]

P(atm)	200 K	220 K	250 K	275 K	300 K
5.00	0.515597	0.571346	0.648050	0.704735	0.754530
2.00	0.615503	0.664443	0.728942	0.774795	0.814022
1.00	0.675785	0.717619	0.772054	0.810475	**0.843277**
0.75	0.695680	0.734781	0.785661	**0.821616**	0.852360
0.50	0.718969	0.754744	**0.801423**	0.834516	0.862887
0.20	0.755734	**0.786230**	0.826338	0.854971	0.879636
0.10	0.773444	0.801417	0.838374	0.864858	0.887729

[a] Figures in bold indicate the approximate temperature−pressure relationship as a function of altitude in the troposphere.

whereas the six d.f. of relative motion were treated as unhindered particle motions with combined $N_{rel.mot.}(E)$ accordingly varying as $E^{(6/2)-1}$.

The probability $P_{A_i}(E_A)$ of formation of acetonoxy rotamer *i* with internal energy E_A is obtained by integrating the expression above over the E_{disp} distribution $F(E_{disp})$; summing over all rotamers *i* gives the probability $P_{form}(E_A)$ of formation of acetonoxy radicals with internal energy E_A. Figures 6 and 7 show the combined $P_{form}(E_A)$ of the acetonoxy radicals for initial reactants at 300 K.

(iv) The resulting acetonoxy radical will either decompose promptly or will be collisionally thermalized. The fraction of prompt dissociation was determined by RRKM-ME analysis, with the $P_{A_i}(E_A)$ obtained above as initial internal energy distribution, using RRKM microcanonical dissociation rates for the oxy rotamers based on the B3LYP-DFT/6-31G(d,p) relative energy and rovibrational data of the transition states and equilibrium structures, and adopting an average energy transferred per collision $\langle\Delta E_{tot}\rangle$ of -130 cm^{-1}. Isomerization is sufficiently fast to maintain microcanonical equilibrium between the various rotamers during dissociation and thermalization. Figure 7 shows the prompt decomposition probability $f(E_A)$ of oxy radicals born with internal energy E_A, for reaction conditions of 300 K and 1 atm. The overall fraction of oxy radicals decomposing promptly is obtained by integrating the product $f(E_A) \times P_{form}(E_A)$ over all energies. For atmospheric conditions, we predict a nearly constant prompt dissociation fraction of about 80% (see Table 4), indicating that the large majority of the acetonoxy radicals formed in (R3) immediately decompose to CH_3CO and CH_2O. A typical population-averaged rate coefficient for prompt decomposition is $\approx 1.3 \times 10^{10}$ s^{-1}. The remainder of the acetonoxy radicals, about 20%, are collisionally thermalized.

The fate of the thermalized acetonoxy radicals, formed either by collisional deactivation of hot acetonoxy radicals from the reaction of acetonylperoxy radicals with NO, or formed in the self-reaction of RO_2 radicals, depends on the competition between thermal dissociation (R5) and reaction with O_2 (R6). The rate of thermal dissociation can be estimated using transition state theory (TST), Troe's low-pressure theory, and Troe's falloff formalism which derives[52,54,55] a temperature- and pressure-dependent rate constant from the high- and low-pressure rate coefficients. In thermal conditions, only the lowest rotamer contributes significantly, with the higher energy rotamer accounting for only 0.16% of the total population even at 300 K. The TST expression for thermal high-pressure rate constants is given by

$$k_\infty = \frac{kT}{h}\cdot\frac{Q^{\neq}}{Q}\cdot e^{-E_0/RT} = \frac{kT}{h}\cdot\frac{Q_{rot}^{\neq}Q_{vib}^{\neq}Q_{el}^{\neq}}{Q_{rot}Q_{vib}Q_{el}}\cdot e^{-E_0/RT} = A_\infty(T)\cdot e^{-E_0/RT}$$

where the barrier height E_0 (=E_b in Figure 6) and partition functions are derived from the DFT quantum chemical calculations. At 300 K, a partition function ratio $Q^{\neq}/Q$ of 2.927 was found, yielding a theoretical preexponential factor A_∞(300 K) of 1.8×10^{13} s^{-1}. Combined with a barrier height of 6.9 kcal/mol, our upper limit estimate, this leads to a high-pressure rate coefficient $k_\infty(300\text{ K}) = 1.7 \times 10^8$ s^{-1}. At 220 K, we find $Q^{\neq}/Q = 2.413$, $A_\infty(220\text{ K}) = 1.1 \times 10^{13}$ s^{-1}, and finally $k_\infty(220\text{ K}) = 1.5 \times 10^6$ s^{-1}. These $k_\infty(T)$ values can be expressed by a formal Arrhenius expression: $k_\infty = 6.72 \times 10^{13} \exp(-3870/T)$ s^{-1}.

The low-pressure limit is calculated using the Troe equation:

$$k_o = kT\cdot Z_{LJ}[M]\beta\frac{N(E_o)e^{-E_0/kT}}{Q_{vib}}F_E F_{anh} F_{rot} F_{int.rot}$$

The Lennard-Jones collision frequency is based on estimated[56,57] collision parameters for the oxy radicals: $\epsilon_{A-A} \approx 400$ K and $\sigma_A = 5$ Å. At 300 K, we find $Z_{LJ}[M] = 1.0 \times 10^{10}$ s^{-1} for N_2 as bath gas. The adopted $\langle\Delta E_{tot}\rangle$ of -130 cm^{-1} can be converted into a collision efficiency $\beta = 0.22$. The vibrational partition function $Q_{vib} = 12.8$ is calculated from the DFT rovibrational data; the vibrational density of states $N(E_0)$ equals 1.2×10^4 states per kcal/mol. The correction factors are all derived from the formulas given by Troe:[52,54,55] $F_E = 1.48$; from the moments of inertia of the minimum and the transition state, $I^{\neq}/I = 1.22$, we derive $F_{rot} = 1.17$; and the anharmonicity correction $F_{anh} = 1.14$. Acetonoxy radicals have 2 degrees of freedom of internal rotation; treating each rotor as an oscillator with an estimated anharmonicity constant of 1.75 we find a correction factor for internal rotation $F_{int.rot} = 3.06$. Thus, at 1 atm and 300 K we find a first-order low-pressure rate coefficient of $k_0(300\text{ K}) = 7.1 \times 10^7$ s^{-1}. At 0.2 atm and 220 K, the parameter values are: $Z_{LJ}[M] = 2.6 \times 10^9$ s^{-1}, $\beta = 0.30$, $Q_{vib} = 5.41$, $F_E = 1.31$, and $F_{rot} = 1.19$; this leads to a first-order low-pressure rate constant of $k_0(220\text{ K}) = 5.6 \times 10^5$ s^{-1}. Then, on the basis of the rate coefficients k_0 and k_∞, and an estimated broadening factor $F_{cent} = 0.5$, we finally obtain a thermal dissociation rate coefficient k_{diss}, listed in Table 5 for different conditions of temperature and pressure.

The yield of $CH_3CO + CH_2O$ from thermalized acetonoxy radicals can then be determined by examining the competition between thermal dissociation and reaction with O_2. Rate coefficients are not known for the latter reaction, but can be estimated from the analogous 1-propoxy radical reaction: $k_{O_2} = 1.4 \times 10^{-14} \exp(-110/T)$ for T = 220−310 K.[35] Table 6

TABLE 5: Rate Constants for Thermal Dissociation of the Acetonoxy Radicals, in the High-pressure Limit and the Falloff Region, Calculated for a Barrier Height to Dissociation of 6.9 Kcal/Mol

P(atm)	200 K	220 K	250 K	275 K	300 K
∞	2.66E+5	1.51E+6	1.24E+7	5.14E+7	1.69E+8
5.00	1.83E+5	9.53E+5	6.59E+6	2.28E+7	6.12E+7
2.00	1.44E+5	7.04E+5	4.47E+6	1.47E+7	3.88E+7
1.00	1.09E+5	5.14E+5	3.17E+6	1.04E+7	**2.73E+7**
0.75	9.55E+4	4.45E+5	2.74E+6	**8.99E+6**	2.33E+7
0.50	7.81E+4	3.63E+5	**2.24E+6**	7.23E+6	1.83E+7
0.20	4.94E+4	**2.27E+5**	1.33E+6	4.03E+6	9.50E+6
0.10	3.39E+4	1.50E+5	8.21E+5	2.36E+6	5.37E+6

TABLE 6: Thermal Dissociation Fraction for the Acetonoxy Radicals at Different Pressures and Temperatures, Calculated Using a Barrier Height to Dissociation of 6.9 Kcal/Mol, Assuming $k_{O2} = k_{1-propoxy+O2}$ (see text), and 20 % O_2[a]

P(atm)	200 K	220 K	250 K	275 K	300 K
5.00	0.382116	0.770951	0.961397	0.989117	0.996136
2.00	0.548344	0.861477	0.976860	0.993233	0.997558
1.00	0.648280	0.900671	0.983556	0.995206	**0.998263**
0.75	0.682313	0.912880	0.985732	**0.995837**	0.998474
0.50	0.725006	0.927687	**0.988306**	0.996548	0.998702
0.20	0.806431	**0.952567**	0.992111	0.997519	0.999002
0.10	0.851298	0.963664	0.993596	0.997886	0.999116

[a] Figures in bold indicate the approximate temperature−pressure relationship as a function of altitude in the troposphere.

TABLE 7: Total Dissociation Fraction at Different Temperatures and Pressures for Acetonoxy Radicals Formed in (R3), Combining Prompt and Thermal Decomposition, Determined Using a Barrier Height to Dissociation of 6.9 Kcal/Mol, Assuming $k_{O2} = k_{1-propoxy+O2}$ (see text), and 20 % O_2

P(atm)	200 K	220 K	250 K	275 K	300 K
5.00	0.70070	0.90182	0.98641	0.99679	0.99905
2.00	0.82634	0.95352	0.99373	0.99848	0.99955
1.00	0.88597	0.97195	0.99625	0.99909	**0.99973**
0.75	0.90332	0.97689	0.99694	**0.99926**	0.99977
0.50	0.92272	0.98226	**0.99768**	0.99943	0.99982
0.20	0.95272	**0.98986**	0.99863	0.99964	0.99988
0.10	0.96631	0.99278	0.99896	0.99971	0.99990

[a] Figures in bold indicate the approximate temperature−pressure relationship as a function of altitude in the troposphere.

lists the dissociation fraction for thermalized acetonoxy radicals in different conditions, with 20% O_2. It is clearly seen that reaction with O_2 is of minimal importance throughout the troposphere, in complete agreement with the experimental findings. The dissociation fractions listed should be considered a lower limit, since they are based on our upper limit estimate of 6.9 kcal/mol for the dissociation barrier height. For high-NO conditions, Table 7 lists the total dissociation fraction by the prompt and thermal decomposition combined; throughout the troposphere, less than 1% of the acetonoxy radicals from acetone are expected to react with O_2 to form methylglyoxal.

No reaction with O_2 was observed in the experiments, even in the absence of NO at 225 K and $P_{O_2} = 650$ Torr ($P_{tot} = 700$ Torr). To verify our estimate for the dissociation barrier height, we redetermined the dissociation fraction theoretically for these conditions. Using a barrier height of 6.9 kcal/mol, our upper limit estimate, we predict 33% formation of $CH_3C(O)CHO$ under the aforementioned conditions, which should still have been detectable. Lowering the barrier height to 6.5 kcal/mol reduces the calculated methylglyoxal yield to about 15%, near the detection limit. These results support our DFT barrier height value of 6.4 kcal/mol. Likewise, our CCSD(T) upper limit of 6.9 kcal/mol is in keeping with the upper limit of 7.5 kcal/mol derived from the experimental data.

Atmospheric Implications

Both the experimental and theoretical results presented above confirm that the rate of dissociation of the acetonoxy radical dominates the rate of its reaction with O_2 at 298 K, as has previously been measured[15,37,58] or estimated from thermodynamic considerations.[17,59] Furthermore, we clearly show that this conclusion also applies for essentially all conditions encountered in the troposphere, even the coldest regions of the upper troposphere. In many regions of the atmosphere, where peroxy radical chemistry is dominated by reaction with NO (e.g., the continental boundary layer and the upper troposphere), this decomposition will in fact occur largely via chemical activation. The energetics involved in the acetonoxy dissociation are similar to those found recently in our laboratories for the 2-hydroxy-1-propoxy species[22] (i.e., a near-thermoneutral dissociation process, a barrier height to decomposition of 6−7 kcal/mol, and a large propensity for prompt, chemically activated dissociation).

The occurrence of acetonoxy radical decomposition reaction, instead of the now ruled-out alternative reaction with O_2, has some minor impacts on both the CH_2O budget and on the HO_x (≡OH + HO_2 + RO_2) production rate in the upper troposphere. Reaction with O_2, followed by the rapid photolysis of methylglyoxal (lifetime ≈ 1 h at 12 km[60]), would lead to the formation of CO, acetylperoxy radicals and HO_2, with a net production of HO_x radicals,

$$CH_3C(O)CH_2O + O_2 \rightarrow CH_3C(O)CHO + HO_2 \quad (6)$$

$$CH_3C(O)CHO + h\nu\ (+\ 2\ O_2) \rightarrow CH_3C(O)O_2 + CO + HO_2$$

$$\text{Net: } CH_3C(O)CH_2O + 3\ O_2 \rightarrow CH_3C(O)O_2 + CO + 2\ HO_2$$

while decomposition leads, of course, to the generation of CH_2O:

$$CH_3C(O)CH_2O\ (+\ O_2) \rightarrow CH_3C(O)O_2 + CH_2O \quad (5)$$

For conditions typical of the upper troposphere,[10] this mechanism accounts for about 10% of the total CH_2O production when acetone levels of 1−2 ppb are encountered (the majority of CH_2O production is via methane oxidation). The formation of CH_2O versus methylglyoxal also acts to suppress HO_x production, since the majority of formaldehyde destruction occurs via non radical-generating processes (mainly photolysis to CO and H_2). However, these effects are likely to be fairly minor (about 10%), given the large rate of HO_x production from the photolysis of acetone itself.

Conclusions

The Cl-atom-initiated oxidation of acetone was studied in an environmental chamber over a range of temperatures, both in the presence and absence of NO_x. No evidence for a reaction of acetonoxy with O_2 was found, and an upper limit to the activation energy for decomposition of the acetonoxy radical, (R5), of 7.5 kcal/mol was obtained. In a theoretical ab initio and statistical kinetics investigation of the acetonoxy decomposition, it was found that the barrier is indeed very low, only 6−7 kcal/mol. Using appropriate and validated methodologies, the chemical activation of acetonoxy radicals from the acetonylperoxy + NO reaction was evaluated, from which it was determined that a large majority of these radicals decompose promptly, under all tropospheric conditions. The dissociation of thermalized acetonoxy radicals was also quantified theoreti-

cally, and was likewise found to be very fast. On the basis of these results, it can be concluded that the chemistry of the acetonoxy radical throughout the troposphere will be dominated by decomposition. In regions where acetonylperoxy radical chemistry is dominated by its reaction with NO (e.g., the continental boundary layer, and the upper troposphere), the internal excitation provided to the acetonoxy species will result in the majority of the decomposition occurring via chemical activation.

Acknowledgment. The National Center for Atmospheric Research is operated by the University Corporation for Atmospheric Research under the sponsorship of the NSF. A portion of this work was supported by the NASA Upper Atmosphere Research Program. The research carried out at Leuven was financially supported by the FWO (Fund for Scientific Research, Flemish Community). L.V. acknowledges the Research Council of the University of Leuven for his BOF Postdoctoral Mandate. Thanks are due to Alex Guenther and Samuel Hall of NCAR for helpful comments on the manuscript.

References and Notes

(1) Duce, R. A.; Mohnen, V. A.; Zimmerman, P. R.; Grosjean, D.; Cautreels, W.; Chatfield, R.; Jaenicke, R.; Ogren, J. A.; Pellizari, E. D.; Wallace, G. T. *Rev. Geophys.* **1983**, *21*, 921.

(2) Arnold, F.; Knop, G.; Zeiereis, H. *Nature* **1986**, *321*, 505.

(3) Möhler, O.; Reiner, Th.; Arnold, F. *Rev. Sci. Instrum.* **1993,** *64*, 1199.

(4) Singh, H. B.; Kanakidou, M.; Crutzen P. J.; Jacob, D. J. *Nature* **1995**, *378*, 50.

(5) Arnold, F.; Schneider, J.; Gollinger, K.; Schlager, H.; Schulte, P.; Hagen, D. E.; Whitefield, P. D.; Van Velthoven, P. *Geophys. Res. Lett.* **1997**, *24*, 57.

(6) Arnold, F.; Bürger, V.; Droste-Fanke, B.; Grimm, F.; Krieger, A.; Schneider, J.; Stilp, T. *Geophys. Res. Lett.* **1997**, *24*, 3017.

(7) Singh, H. B.; O'Hara, D.; Herlth, D. Sachse, G. W.; Blake, D. R.; Bradshaw, J. D.; Kanakidou, M.; Crutzen P. J. *J. Geophys. Res.* **1994**, *99*, 1805.

(8) Orlando, J. J.; Nozière, B.; Tyndall, G. S.; Paulson, S. E.; Orzechowska, G.; Rudich, Y. *J. Geophys. Res.* **2000**, *105*, 11561.

(9) Jobson, B. T.; Niki, H.; Yokouchi, Y.; Bottenheim, J.; Hopper, F.; Leaitch, R., *J. Geophys. Res.* **1994**, *99*, 25355.

(10) McKeen, S. A.; Gierczak, T.; Burkholder, J. B.; Wennberg, P. O.; Hanisco, T. F.; Keim, E. R.; Gao, R. S.; Liu, S. C.; Ravishankara, A. R.; Fahey, D. W. *Geophys. Res. Lett.* **1997**, *24*, 3177.

(11) Wennberg, P. O.; et al. *Science* **1998**, *279*, 49.

(12) Müller, J.-F.; Brasseur, G. *J. Geophys. Res.* **1999**, *104*, 1705.

(13) Wollenhaupt, M.; Carl, S. A.; Horowitz, A.; Crowley, J. N. *J. Phys. Chem. A* **2000**, *104*, 2695.

(14) Wollenhaupt, M.; Crowley, J. N. *J. Phys. Chem. A* **2000**, *104*, 6429.

(15) Jenkin, M. E.; Cox, R. A.; Emrich, M.; Moortgat, G. K. *J. Chem. Soc., Faraday Trans.* **1993**, *89*, 2983.

(16) Bridier, I.; Veyret, B.; Lesclaux, R.; Jenkin, M. E. *J. Chem. Soc., Faraday Trans.* **1993**, *89*, 2993.

(17) Atkinson, R.; Carter, W. P. L. *J. Atmos. Chem.* **1991**, *13*, 195.

(18) Sehested, J.; Christensen, L. K.; Nielsen, O. J.; Bilde, M.; Wallington, T. J.; Schneider, W. F.; Orlando, J. J.; Tyndall, G. S. *Int. J. Chem. Kinet.* **1998**, *30*, 475.

(19) Wallington, T. J.; Hurley, M. D.; Fracheboud, J. M.; Orlando, J. J.; Tyndall, G. S.; Sehested, J.; Møgelberg, T. E.; Nielsen O. J. *J. Phys. Chem.* **1996**, *100*, 18116.

(20) Orlando, J. J.; Tyndall, G. S.; Bilde, M.; Ferronato, C.; Wallington, T. J.; Vereecken, L.; Peeters, J. *J. Phys. Chem. A* **1998**, *102*, 8116.

(21) Vereecken, L.; Peeters, J. *J. Phys. Chem. A* **1999**, *103*, 1768.

(22) Vereecken, L.; Peeters, J.; Orlando, J. J.; Tyndall, G. S.; Ferronato, C. *J. Phys. Chem. A* **1999**, *103*, 4693.

(23) Schneider, W. F.; Wallington, T. J.; Barker, J. R.; Stahlberg, E. A. *Ber. Bunsen-Ges. Phys. Chem.* **1998**, *102*, 1850.

(24) Lightfoot, P. D.; Cox, R. A.; Crowley, J. N.; Destriau, M.; Hayman, G. D.; Jenkin, M. E.; Moortgat, G. K.; Zabel, F. *Atmos. Environ.* **1992**, *26A*, 1805.

(25) Shetter, R. E.; Davidson, J. A.; Cantrell, C. A.; Calvert, J. G. *Rev. Sci. Instrum.* **1987**, *58*, 1427.

(26) Orlando, J. J. *Int. J. Chem. Kinet.* **1999**, *31*, 515.

(27) Wallington, T. J.; Andino, J. M.; Ball, J. C.; Japar, S. M. *J. Atmos. Chem.* **1990**, *10*, 301.

(28) Shi, J.; Wallington, T. J.; Kaiser, E. W. *J. Phys. Chem.* **1993**, *97*, 6184.

(29) Christensen, L. K.; Ball, J. C.; Wallington T. J. *J. Phys. Chem. A* **2000**, *104*, 345.

(30) Crawford, M. A.; Wallington, T. J.; Szente, J. J.; Maricq, M. M.; Francisco, J. S. *J. Phys. Chem. A* **1999**, *103*, 365.

(31) Niki, H.; Maker, P. D.; Savage, C. M.; Breitenbach, L. P. *J. Phys. Chem.* **1985**, *89*, 588.

(32) Moortgat, G. K.; Veyret, B.; Lesclaux, R. *Chem. Phys. Lett.* **1989**, *160*, 443.

(33) Horie, O.; Moortgat, G. K. *J. Chem. Soc., Faraday Trans* **1992**, *88*, 3305.

(34) Notario, A.; Mellouki, A.; Le Bras, G. *Int. J. Chem. Kinet.* **2000**, *32*, 62.

(35) Atkinson, R.; Baulch, D. L.; Cox, R. A.; Hampson, R. F., Jr.; Kerr, J. A.; Rossi, M. J.; Troe, J. *J. Phys. Chem. Ref. Data* **1997**, *26*, 521.

(36) Braun, W.; Herron, J. T.; Kahaner, D. K. *Int. J. Chem. Kinet.* **1988**, *20*, 51.

(37) Sehested, J.; Christensen, L. K.; Nielsen, O. J.; Bilde, M.; Wallington, T. J.; Schneider, W. F.; Orlando, J. J.; Tyndall, G. S. *Int. J. Chem. Kinet.* **1998**, *30*, 475.

(38) DeMore, W. B.; Sander, S. P.; Golden, D. M.; Hampson, R. F.; Kurylo, M. J.; Howard, C. J.; Ravishankara, A. R.; Kolb, C. E.; Molina, M. J. Chemical Kinetics and Photochemical Data for Use in Stratospheric Modeling; Evaluation #12, 1997, JPL Publication 97-04, Pasadena CA.

(39) Tyndall, G. S.; Cox, R. A.; Granier, C.; Lesclaux, R.; Moortgat, G. K.; Pilling, M. J.; Ravishankara, A. R.; Wallington, T. J. *J. Geophys. Res.* **2000**, submitted.

(40) Maricq, M. M.; Szente, J. J.; Kaiser, E. W.; Shi, J. *J. Phys. Chem.* **1994**, *98*, 2083.

(41) Helleis, F.; Crowley, J. N.; Moortgat, G. K. *J. Phys. Chem.* **1993**, *97*, 11464.

(42) Atkinson, R. *Int. J. Chem. Kinet.* **1997**, *29*, 99.

(43) Blitz, M.; Pilling, M. J.; Robertson, S. H.; Seakins, P. W. *Phys. Chem. Chem. Phys* **1999**, *1*, 73.

(44) Caralp, F.; Devolder, P.; Fittschen, C.; Gomez, N.; Hippler, H.; Méreau, R.; Rayez, M. T.; Striebel, F.; Viskolcz, B. *Phys. Chem. Chem. Phys.* **1999**, *1*, 2935.

(45) Orlando, J. J.; Iraci, L. T.; Tyndall, G. S. *J. Phys. Chem. A* **2000**, *104*, 5072.

(46) Frisch, M. J.; Trucks, G. W.; Schlegel, H. B.; Scuseria, G. E.; Robb, M. A.; Cheeseman, J. R.; Zakrzewski, V. G.; Montgomery, J. A., Jr.; Stratmann, R. E.; Burant, J. C.; Dapprich, S.; Millam, J. M.; Daniels, A. D.; Kudin, K. N.; Strain, M. C.; Farkas, O.; Tomasi, J.; Barone, V.; Cossi, M.; Cammi, R.; Mennucci, B.; Pomelli, C.; Adamo, C.; Clifford, S.; Ochterski, J.; Petersson, G. A.; Ayala, P. Y.; Cui, Q.; Morokuma, K.; Malick, D. K.; Rabuck, A. D.; Raghavachari, K.; Foresman, J. B.; Cioslowski, J.; Ortiz, J. V.; Stefanov, B. B.; Liu, G.; Liashenko, A.; Piskorz, P.; Komaromi, I.; Gomperts, R.; Martin, R. L.; Fox, D. J.; Keith, T.; Al-Laham, M. A.; Peng, C. Y.; Nanayakkara, A.; Gonzalez, C.; Challacombe, M.; Gill, P. M. W.; Johnson, B. G.; Chen, W.; Wong, M. W.; Andres, J. L.; Head-Gordon, M.; Replogle, E. S.; Pople, J. A. *Gaussian 98*, revision A.5; Gaussian, Inc.: Pittsburgh, PA, 1998.

(47) Scott, A. P.; Radom, L. *J. Phys. Chem.* **1996**, *100*, 16502.

(48) Mereau, R.; Rayez, M. T.; Caralp, F.; Jimeno, P.; Rayez, J. C.; Gomez, N.; Fittschen, C. 15th International Symposium on Gas Kinetics, Bilbao, 1998, poster A32, Book of Abstracts, p 134.

(49) Vereecken, L.; Huyberechts, G.; Peeters, J. *J. Chem. Phys.* **1997**, *106*, 6564.

(50) Forst, W. *Theory of Unimolecular Reactions*; Academic Press: New York, 1973.

(51) Jungkamp, T. P. W.; Smith, J. N.; Seinfeld, J. H. *J. Phys. Chem. A* **1997**, *101*, 1973.

(52) Troe, J. *J. Chem. Phys.* **1977**, *66*, 4745.

(53) Wittig, C.; Nadler, I.; Reisler, H.; Noble, M.; Catanzarite, J.; Radhakrishnan, G. *J. Chem. Phys.* **1985**, *83*, 5581.

(54) Troe, J. *J. Chem. Phys.* **1977**, *66*, 4758.

(55) Troe, J. *J. Phys. Chem.* **1979**, *83*, 114.

(56) Oref, I.; Tardy, D. C. *Chem. Rev.* **1990**, *90*, 1407.

(57) Hirschfelder, J. O.; Curtiss, C. F.; Bird, R. B. *Molecular Theory of Gases and Liquids*; John Wiley & Sons: New York, 1967.

(58) Cox, R. A.; Patrick, K. F.; Chant, S. A. *Environ. Sci. Technol.* **1981**, *15*, 587.

(59) Baldwin, A. C.; Barker, J. R.; Golden, D. M.; Hendry, D. G. *J. Phys. Chem.* **1977**, *81*, 2483.

(60) Koch, S.; Moortgat, G. K. *J. Phys. Chem. A* **1998**, *102*, 9142.